

# Research & Reviews: Journal of Chemistry

## Nano-Crystalline $\text{Co}_3\text{O}_4$ Spinel Prepared by Combustion Method as a Catalyst for Direct Decomposition of $\text{N}_2\text{O}$

Makhlouf MT, Abu-Zied BM, Mansoure TH and Ibrahim SA\*

Chemistry Department, Faculty of Science, Assiut University, 71516 Assiut, Egypt

### RESEARCH ARTICLE

Received date: 12/08/2015

Accepted date: 12/11/2015

Published date: 16/11/2015

#### \*For Correspondence

Ibrahim SA, Chemistry Department, Faculty of Science, Assiut University, Assiut, Egypt, Tel: +201227442799

E-mail: saidib@aun.edu.eg/saidibrahim7@yahoo.com

**Keywords:**  $\text{N}_2\text{O}$  decomposition, Nano-crystalline  $\text{Co}_3\text{O}_4$ , Combustion.

#### ABSTRACT

Combustion method has been used as a fast and facile method to prepare nano-crystalline  $\text{Co}_3\text{O}_4$  spinel employing urea as a combustion fuel. Alkali-promoted catalysts were prepared by the incipient wetness impregnation of the prepared nano-material with the aqueous solutions of alkali carbonates ( $\text{Li}_2\text{CO}_3$ ,  $\text{Na}_2\text{CO}_3$ ,  $\text{K}_2\text{CO}_3$ , and  $\text{Cs}_2\text{CO}_3$ ).  $\text{N}_2\text{O}$  decomposition was investigated over pure and alkali promoted nano-crystalline  $\text{Co}_3\text{O}_4$  catalysts. The beneficial influence of dopants on the catalyst activity increases in the order: un-promoted  $<\text{Li}<\text{Na}<\text{K}<\text{Cs}$ . The effects of changing the Cs/Co molar ratio and calcination temperature on the catalyst activity were also examined. The results showed that the enhancement was critically dependent upon the amount of Cs and the calcination temperature. Thermal analyses (TGA and DTA), X-ray diffraction technique (XRD),  $\text{N}_2$ -adsorption and FTIR techniques were used to characterize the prepared catalysts.

### INTRODUCTION

Nitrous oxide ( $\text{N}_2\text{O}$ ) is a dangerous environmental pollutant because of its high greenhouse potential and its ozone-depleting property [1]. The Kyoto Protocol of the United Nations Convention on Climate Change (December 1997) cited  $\text{N}_2\text{O}$  as a second non- $\text{CO}_2$  greenhouse gas.  $\text{N}_2\text{O}$  is a greenhouse gas with a long life time of about 150 years in the atmosphere [2,3]. Although  $\text{N}_2\text{O}$  is not the major contributor to global warming, it is much more potent than either of the other two most common anthropogenic greenhouse gases,  $\text{CO}_2$  and  $\text{CH}_4$ .  $\text{N}_2\text{O}$  is 310 and 21 times of the Global warming potential (GWP) of  $\text{CO}_2$  and  $\text{CH}_4$ , respectively [2,4]. Furthermore,  $\text{N}_2\text{O}$  is an important source of stratospheric nitrogen oxides, which initiates a chain of cyclic reaction leading to stratospheric ozone destruction [2-5]. It is emitted from both natural and anthropogenic sources such as nitric acid and adipic acid plants and fluidized bed combustors for sewage-sludge or industrial wastes besides the medical exhaust as well as biological and agricultural emissions [6]. The concentration of nitrous oxide in the atmosphere continues to increase, and this increase appears to be caused mainly by human activities. With increasing concerns about protecting our environment, the catalytic removal of nitrous oxide from exhausts becomes very attractive [7].

Heterogeneous catalytic decomposition of  $\text{N}_2\text{O}$  to its elements nitrogen and oxygen, is a suitable solution in many of the anthropogenic emission sources, and various catalytic formulations have been proposed, including supported and unsupported metals [8-11], pure and mixed oxides [12-15] and zeolites [16-19]. Supported noble metal catalysts, such as Rh catalysts [4], show high activities in  $\text{N}_2\text{O}$  decomposition reactions at 200-300 °C. However, the high cost of the noble metal limits their applications. Transition metal ion exchanged zeolite catalysts such as Fe-ZSM-5 are more active in the selective catalytic reduction (SCR) of  $\text{N}_2\text{O}$  by hydrocarbons than in the decomposition of  $\text{N}_2\text{O}$  in a temperature range of 300-400 °C [3]. Recently, spinel-type oxides have been a subject of increasing applied research [20-24] in addition to be used as efficient catalysts [25-28]. Among them cobalt oxide,  $\text{Co}_3\text{O}_4$ , which belongs to the family of complex-metal oxides known as spinels.  $\text{Co}_3\text{O}_4$  adopt the normal spinel crystal structure based on a cubic close packing array of oxide atoms which have the general formula  $\text{AB}_2\text{O}_4$  in which A is a divalent cation located at the tetrahedral 8a sites, and B atoms are trivalent cations occupying the octahedral 16d sites. Cobalt containing spinels was shown

to be superior to other transition metal spinels towards the  $N_2O$  decomposition in presence or in absence of oxygen [7,9,13,15].  $Co_3O_4$  received paid attention due to its promising applications in gas sensing [20], low temperature CO oxidation [21], anode materials in Li-ion batteries [22], steam reforming of ethanol [23], oxidation of volatile organic compounds (VOCs) [24],  $N_2O$  decomposition [25], ammonia oxidation [26], Fischer-Tropsch synthesis (FTS) [27], and decomposition of hydrogen peroxide [28,29]. Much effort has been directed to prepare  $Co_3O_4$  nano-particles, including sol-gel [30], hydrothermal [31], micro-emulsion [32], microwave-assisted hydrothermal [33], and combustion synthesis [29,34,35].

Recent studies indicated that the residual alkali metals in the Co-based catalysts, which were introduced during the precipitation, caused a significant increase of catalytic activity [36]. For example, Stelmachowski *et al.* [37] studied the  $N_2O$  decomposition over alkali-doped  $Co_3O_4$  and found that the addition of alkali-promoters greatly enhance the catalytic activity for  $N_2O$  decomposition in the order:  $Li < Na < K < Cs$ . In addition, Ohnishi *et al.* [38] found that the sodium content remaining in the  $Co_3O_4$  catalyst was the determining factor controlling the activity and the optimal Na/Co molar ratio was  $3.8 \times 10^{-3}$ . Similarly, it is observed that the presence of residual K in  $Co_3O_4-CeO_2$  which was prepared by co-precipitation with  $K_2CO_3$  as the precipitant improved largely the catalytic performance [39]. Motivated by these experimental findings, Asano *et al.* [7] prepared K-doped  $Co_3O_4$  catalyst by impregnation of  $KNO_3$  on  $CoCO_3$ , in which the alkali content could be finely tuned. They concluded that the number of active sites increased and desorption of oxygen was promoted by the addition of K to the  $Co_3O_4$ , which resulted in an enhanced activity for  $N_2O$  decomposition. In addition to the promotional effect of Na and K on  $Co_3O_4$  catalyst, it is also observed that the addition of an appropriate amount of Cs to  $Co_3O_4$  could weaken the Co-O bond, and the Cs-modified  $Co_3O_4$  catalyst exhibited higher activity for  $N_2O$  decomposition compared to bulk  $Co_3O_4$  [40].

In the present work,  $N_2O$  decomposition over bulk and alkali promoted (Li, Na, K and Cs) nano-crystalline  $Co_3O_4$  catalysts, prepared using combustion method, was studied. We found that the catalyst activity increases in the order: unpromoted  $< Li < Na < K < Cs$ . Our study was extended to check the effect of changing both the Cs/Co molar ratio and calcination temperature on the catalyst activity towards  $N_2O$  decomposition.

## EXPERIMENTAL

### Preparation Procedure

The nano-crystalline  $Co_3O_4$  was prepared using the combustion method as described elsewhere [29]. Urea was used as a combustion fuel. In a typical procedure, the required amounts of cobalt nitrate and urea for urea/cobalt nitrate molar ratio of 8 were weighed to the nearest milligram. Cobalt nitrate and urea were dissolved in 100 mL of distilled water to form a pink homogeneous solution; the solution was then transferred to a flask fitted with a water condenser, after that it was heated to  $100^\circ C$  with stirring. The reaction mixture was refluxed with stirring at that temperature for 12 hours. The product obtained was evaporated by heating over a hotplate at  $100^\circ C$ . Finally, the dried precursor was calcined in a Muffle furnace at  $400^\circ C$  for 3 hour in a static air atmosphere.

Alkali-doped catalysts were prepared by the incipient wetness impregnation of prepared nano-crystalline  $Co_3O_4$  with the aqueous solutions of alkali carbonates ( $Li_2CO_3$ ,  $Na_2CO_3$ ,  $K_2CO_3$ , and  $Cs_2CO_3$ ). The alkali carbonates were found to be more efficient precursors than the corresponding hydroxides [41]. Three series of samples were prepared. In the first one (series I), we have investigated the influence of adding alkali cations ( $Li^+$ ,  $Na^+$ ,  $K^+$ , and  $Cs^+$ ) in promotion of  $N_2O$  decomposition. The alkali metal/cobalt ratio was adjusted to 0.05. The obtained mixtures were dried at  $90^\circ C$  overnight and then calcined at  $400^\circ C$  for 3 h in a static air atmosphere. Based on  $N_2O$  measurements, in series II, we have investigated the influence of changing Cs/Co ratio, from 0.0125 – 0.200, on the catalysts activity towards  $N_2O$  decomposition. After that, In order to investigate the effect of calcination temperature, in series III, we calcined the most active sample, i.e., Cs/ $Co_3O_4$  with Cs/Co 0.025 molar ratio, at different temperatures (i.e.,  $500^\circ C$ ,  $600^\circ C$  and  $700^\circ C$ ).

### Characterization

Simultaneous TGA and DTA curves were recorded with a Shimadzu DTG-60 apparatus using a heating rate of  $10^\circ C \text{ min}^{-1}$  in air atmosphere (flow rate 40 ml/min). Powder X-ray diffraction (XRD) patterns were recorded using Philips diffractometer (Type PW 103/00) with  $CuK\alpha$  radiation ( $\lambda=1.5405 \text{ \AA}$ ) at 35 kV and 20 mA with a scanning rate in  $2\theta$  of  $0.06 \text{ min}^{-1}$ . FTIR spectra were performed as KBr discs in the range  $4000-400 \text{ cm}^{-1}$ , using Thermo-Nicolet-6700 FTIR spectrophotometer. BET surface areas were determined on a Quantachrome (Nova 3200 series) multi-gas adsorption instrument with nitrogen physisorption at  $-196^\circ C$ .

### Activity Measurements

The catalytic reaction was carried out in a fixed-bed quartz flow reactor, containing approximately 500 mg of the catalyst in all the experiments. The temperature in the reactor was measured using a thermocouple on the catalyst bed and was controlled within  $\pm 0.2^\circ C$  of the desired temperature by a Cole-Parmer temperature controller (model Digi-Sense 89000-00). The desired concentration of  $N_2O$  was added with the aid of thermal mass flow controllers (AALBORG, DFC2600) using  $N_2$  as a balance gas, the volume flow rate was  $200 \text{ cm}^3/\text{min}$  (NTP). Analysis of the reactor inlet and outlet gases was carried out using a magnetic oxygen analyzer (ABB, AO2020-Magnos 106) and non-dispersive infrared analyzer for the components  $N_2O$  and NO (ABB, AO2020-Uras

14). Preliminary experiments for the decomposition of nitrous oxide over all the catalysts showed the absence of NO in the exit gas.

## RESULTS AND DISCUSSION

### Catalysts Characterization

**Thermal analysis:** Figure 1 shows the TG profiles, in air atmosphere as a carrier gas, of the calcined precursors (alkali-promoted  $\text{Co}_3\text{O}_4$  with alkali/Co ratio 0.05) at  $400^\circ\text{C}$ , all of which showed essentially the same profile, and two weight-decrease processes were observed at the temperature ranges of  $50\text{--}280^\circ\text{C}$  and  $740\text{--}900^\circ\text{C}$ . The former is due to dehydration of the adsorbed water, and the latter weight decrease is attributed to decomposition of the alkali-carbonates, releasing  $\text{CO}_2$ , and thermal reduction of  $\text{Co}_3\text{O}_4$  to  $\text{CoO}$  [29,34,35].

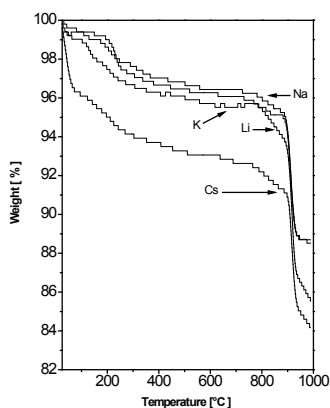


**Figure 1.** Thermal decomposition behavior of the precursors (alkali-promoted nano-crystalline  $\text{Co}_3\text{O}_4$  having alkali/Co ratio 0.05) calcined at  $400^\circ\text{C}$ .

**X-ray diffraction:** XRD patterns of un-promoted (a); and alkali-promoted ( $\text{Li}^+$  (b),  $\text{Na}^+$  (c),  $\text{K}^+$  (d), and  $\text{Cs}^+$  (e)) nano-crystalline  $\text{Co}_3\text{O}_4$  catalysts having alkali/cobalt ratio of 0.05 being calcined at  $400^\circ\text{C}$  are shown in Figure 2. Only nano-crystalline  $\text{Co}_3\text{O}_4$  spinel phase and no alkali-containing components can be observed due to the low content and mono-layer dispersion of alkali species on catalyst surface. The line profile, shown in Figure 2, is fitted for 8 peaks for nano-crystalline  $\text{Co}_3\text{O}_4$  (JCPDS no. 80-1545) ( $2\theta=18.94^\circ$ ,  $31.30^\circ$ ,  $36.82^\circ$ ,  $38.50^\circ$ ,  $44.80^\circ$ ,  $55.66^\circ$ ,  $59.38^\circ$ ,  $65.20^\circ$ ) [34], marked by their indices planes [(111), (220), (311), (222), (400), (422), (511), (440)], respectively. The peaks became broader by the addition of alkali-cations but no peak shift was observed, indicating that alkali-cations are highly dispersed in the matrix of the nano-crystalline  $\text{Co}_3\text{O}_4$  catalyst [7]. In addition, the intensities of the XRD peaks related to the nano-crystalline  $\text{Co}_3\text{O}_4$  reflections are slightly decreased. The crystallite sizes (D) of alkali-doped nano-crystalline  $\text{Co}_3\text{O}_4$  were calculated using Scherrer equation [35] from the full-width at half-maximum (FWHM) of the peak at  $2\theta=36.82^\circ$ . The relevant values are listed in Table 1. From Table 1, it is evident that the  $\text{Li}/\text{Co}_3\text{O}_4$  (0.05) catalyst had the largest  $\text{Co}_3\text{O}_4$  crystallites, followed by the  $\text{Na}/\text{Co}_3\text{O}_4$  (0.05) and  $\text{K}/\text{Co}_3\text{O}_4$  (0.05) catalysts, while the  $\text{Cs}/\text{Co}_3\text{O}_4$  (0.05) catalyst had rather small crystallites. Therefore, and based on  $\text{N}_2\text{O}$  activity, our study was extended to check the influence of changing the  $\text{Cs}/\text{Co}^{2+}$  molar ratio on the crystallite size and  $\text{N}_2\text{O}$  decomposition activity of Cs-promoted  $\text{Co}_3\text{O}_4$ .

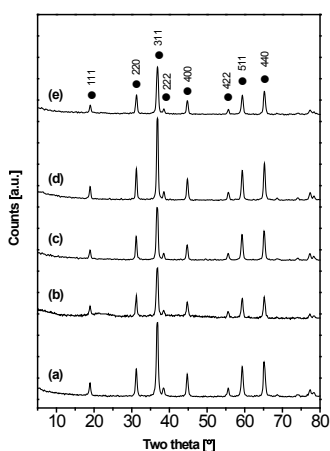


**Figure 2.** XRD spectra of un-promoted (a); and alkali-promoted ( $\text{Li}^+$  (b),  $\text{Na}^+$  (c),  $\text{K}^+$  (d), and  $\text{Cs}^+$  (e)) nano-crystalline  $\text{Co}_3\text{O}_4$  catalysts having alkali/cobalt ratio of 0.05 being calcined at  $400^\circ\text{C}$ .

XRD patterns of the Cs promoted nano-crystalline  $\text{Co}_3\text{O}_4$  with different Cs/Co ratios are shown in Figure 3. XRD pattern of the samples shows only the characteristic peaks of nano-crystalline  $\text{Co}_3\text{O}_4$  at lower Cs/ $\text{Co}^{2+}$  ratios (i.e.,  $<0.1$ ). While, at higher Cs/ $\text{Co}^{2+}$  ratios, peaks due to the crystalline  $\text{Cs}_2\text{CO}_3$  phases (JCPDS no. 71-1981) are noticed, in addition to  $\text{Co}_3\text{O}_4$ . The intensity of

these peaks was found to increase with increasing Cs loading. The XRD patterns suggest that at higher Cs content the crystallites of  $\text{Cs}_2\text{CO}_3$  are formed on the surface of  $\text{Co}_3\text{O}_4$ .

**Table 1.** Physico-chemical properties of alkali-promoted nano-crystalline  $\text{Co}_3\text{O}_4$  catalysts.

Catalysts	Crystallite Size (nm)	$S_{\text{BET}}$
Li/ $\text{Co}_3\text{O}_4$ (0.05)	22	25.35
Na/ $\text{Co}_3\text{O}_4$ (0.05)	19.8	25.44
K/ $\text{Co}_3\text{O}_4$ (0.05)	19.6	20.57
Cs/ $\text{Co}_3\text{O}_4$ (0.05)	19	23.9
Cs/ $\text{Co}_3\text{O}_4$ (0.0125)	19.9	29.05
Cs/ $\text{Co}_3\text{O}_4$ (0.025)	17	34
Cs/ $\text{Co}_3\text{O}_4$ (0.1)	21	19.2
Cs/ $\text{Co}_3\text{O}_4$ (0.2)	23	11.97
Cs/ $\text{Co}_3\text{O}_4$ (0.025) - 500 °C	20.3	11.2
Cs/ $\text{Co}_3\text{O}_4$ (0.025) - 600 °C	22.9	3.77
Cs/ $\text{Co}_3\text{O}_4$ (0.025) - 700 °C	24.8	2.70

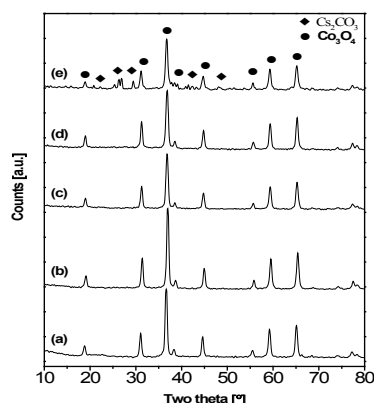


**Figure 3.** XRD spectra of cesium-promoted (0.0125 (a), 0.025 (b), 0.05 (c), 0.1 (d), and 0.2 (e))  $\text{Co}_3\text{O}_4$  catalysts being calcined at 400 °C.

In order to check the role of Cs/ $\text{Co}^{2+}$  ratio in changing the structural parameters of nano-crystalline  $\text{Co}_3\text{O}_4$  such as lattice parameter (a) and crystallite size (D), the lattice parameters were computed using the *d*-spacing values and the respective (hkl) parameters. The obtained results are plotted in **Figure 4**. The variation of the lattice parameter with Cs/ $\text{Co}^{2+}$  ratio follows the same trend as that observed for the crystallite size. Inspection of **Figure 4** revealed that, the crystallite size of Cs/ $\text{Co}_3\text{O}_4$  decreased with increasing the cesium/cobalt ratio from 0.0125 till 0.025, and then it shows a mild continuous increase upon further Cs/ $\text{Co}^{2+}$  increase.

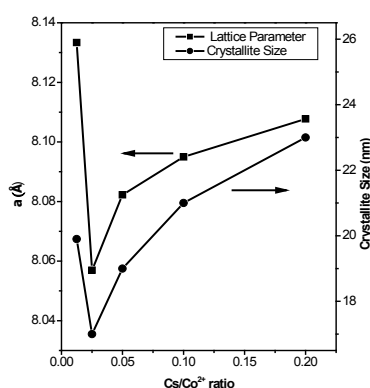


**Figure 4.** Effect of Cs/Co ratio on the lattice parameter and crystallite size values of nano-crystalline  $\text{Co}_3\text{O}_4$  catalysts being calcined at 400 °C.

Since the Cs/ $\text{Co}_3\text{O}_4$  obtained by using Cs/ $\text{Co}^{2+}$  ratio of 0.025 exhibits the lowest crystallite size, the study was extended to check the influence of changing the calcination temperature on the crystallite size of Cs-promoted nano-crystalline  $\text{Co}_3\text{O}_4$  at this ratio. XRD patterns of the as-prepared Cs/ $\text{Co}_3\text{O}_4$  obtained via calcining Cs/ $\text{Co}^{2+}$  parents having molar ratio of 0.025 at 400-700 °C temperature range are shown in **Figure 5**. From this figure four points could be raised: (i) all diffraction peaks belong to one phase only ( $\text{Co}_3\text{O}_4$ ) at the calcination temperatures range 400-700 °C, (ii) these peaks showed a continuous decrease in their intensities with increasing the calcination temperature, (iii) No Cs-containing phase was found possibly due to the low content and mono-layer dispersion of Cs species on catalyst surface, and (iv) the diffraction peaks for Cs doped  $\text{Co}_3\text{O}_4$  shift continuously to lower  $2\theta$  values upon increasing the calcination temperature from 400 till 700 °C, indicating an increase in the spinel lattice parameters, characteristic for formation of a solid solution [42]. **Figure 6** shows the lattice parameters of nano-crystalline  $\text{Co}_3\text{O}_4$  phase at different calcination temperatures (400-700 °C) and the crystallite size calculated from XRD data. From these data one

can state safely that, the sample calcined at 400 °C exhibits the lowest crystallite size ( $D=17$  nm). With increasing the calcination temperature the average crystallite size is increased. This behavior is expected because the heating facilitates the diffusion and agglomeration of the particles.

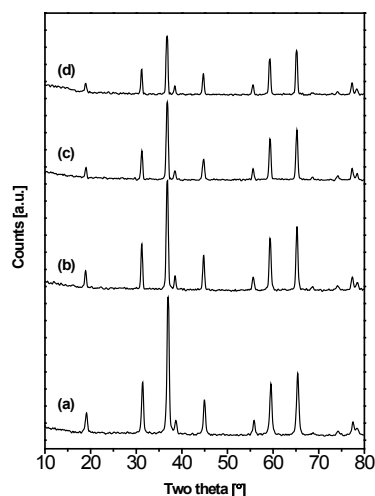


**Figure 5:** XRD spectra of cesium-promoted (400 °C (a), 500 °C (b), 600 °C (c), and 700 °C (d))  $\text{Co}_3\text{O}_4$  catalysts having cesium/cobalt ratio of 0.025.

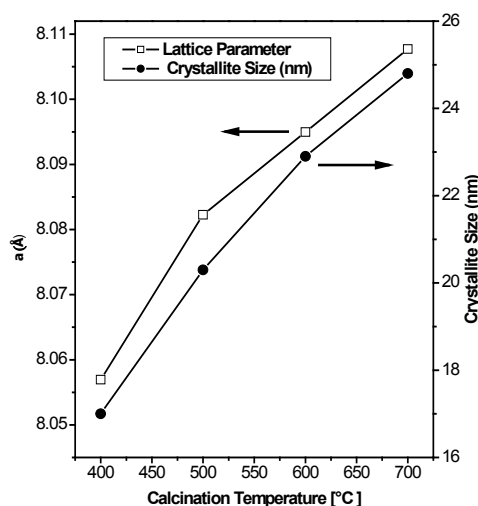


**Figure 6.** Effect of calcination temperature on the lattice parameter and crystallite size values of  $\text{Cs}/\text{Co}_3\text{O}_4$  catalyst, having  $\text{Cs}/\text{Co}$  0.025, being calcined at 400 °C.

**Fourier Transformation Infrared Spectroscopy (FTIR):** Cubic spinel structure of  $\text{Co}_3\text{O}_4$  with  $\text{Co}^{2+}$  ( $3d^7$ ) and  $\text{Co}^{3+}$  ( $3d^6$ ) located at tetrahedral and octahedral sites, respectively, belongs to the space group ( $Fd\bar{3}m$ )<sup>[34]</sup>. The group theory predicts the following modes in the spinel<sup>[35]</sup>:  $\Gamma=A_{1g}(R)+E_g(R)+F_{1g}(\text{in})+3F_{2g}(R)+2A_{2u}(\text{in})+2E_u(\text{in})+4F_{1u}(\text{IR})+2F_{2u}(\text{in})$ , where (R), (IR) and (in) represent Raman active vibrations, infrared-active vibration and inactive modes, respectively. The FTIR spectra of un-promoted and alkali-promoted nano-crystalline  $\text{Co}_3\text{O}_4$  catalyst (alkali= $\text{Li}^+$ ,  $\text{Na}^+$ ,  $\text{K}^+$  and  $\text{Cs}^+$  where alkali/ $\text{Co}^{2+}$  molar ratio=0.05), being calcined at 400 °C are shown in **Figure 7**. In the investigated region ( $4000\text{--}400\text{ cm}^{-1}$ ), the entire obtained spectra manifest the presence of two absorption bands at  $567(\nu_1)$  and  $662(\nu_2)\text{ cm}^{-1}$ ; which originate from the stretching vibrations of the metal-oxygen bond and confirm the formation of  $\text{Co}_3\text{O}_4$  spinel oxide<sup>[34,35]</sup>. The  $\nu_1$  band is characteristic of  $\text{OB}_3$  (where B denotes the  $\text{Co}^{3+}$  in the octahedral hole) vibration and the  $\nu_2$  band is attributable to the  $\text{ABO}_3$  (where A denotes the  $\text{Co}^{2+}$  in the tetrahedral hole) vibration in the spinel lattice. The intensities of such peaks decreased and became broader upon the addition of alkali-cations. For the un-promoted nano-crystalline  $\text{Co}_3\text{O}_4$  catalyst, **Figure 7** shows a broad band centered at  $3400\text{ cm}^{-1}$  and an absorption band at  $1630\text{ cm}^{-1}$ , such absorption were assigned to the O-H stretching and bending modes of water<sup>[32]</sup>, respectively, which indicates that the surface was hydroxylated because the sample was exposed to air and some water was adsorbed probably on the external surface of the samples during handling to record the spectra. For alkali-promoted nano-crystalline  $\text{Co}_3\text{O}_4$ , one can observe another set of absorption bands at  $858, 1155$  and  $1523\text{ cm}^{-1}$  corresponding to the different vibration modes of carbonate anion<sup>[25,33]</sup>. The band at  $2360\text{ cm}^{-1}$  was assigned to vibration of carbon dioxide molecule<sup>[33]</sup>.

**Figure 8** shows the FT-IR spectra of  $\text{Cs}/\text{Co}_3\text{O}_4$  catalysts ( $\text{Cs}/\text{Co}=0.0125, 0.025, 0.05, 0.1, 0.2$ ), being calcined at 400 °C. Also, all the obtained spectra manifest the presence of two strong absorptions at  $567$  and  $662\text{ cm}^{-1}$ . Such absorptions were assigned, respectively, to  $\nu_1$  and  $\nu_2$  stretching vibrations of the metal-oxygen bond in  $\text{Co}_3\text{O}_4$  spinel oxide<sup>[34]</sup>. Moreover, one can observe another set of absorptions at  $1400\text{--}1550\text{ cm}^{-1}$ . Such absorptions was assigned, again, to vibration mode of carbonate

anion <sup>[25,33]</sup>. In this context, it is worth mentioning that the intensity of such absorption increases with increasing Cs/Co<sup>2+</sup> molar ratio. At Cs/Co<sup>2+</sup> molar ratio of 0.2, there are another two additional bands at 1008 and 831 cm<sup>-1</sup>; also this can be assigned to the carbonate anion. For the same series of catalysts, **Figure 8** shows absorption at 1668 cm<sup>-1</sup>, this can be assigned to the H-O-H bending mode of vibration <sup>[32]</sup>. The band at 2360 cm<sup>-1</sup> was assigned to vibration of CO<sub>2</sub> molecule <sup>[33]</sup>.

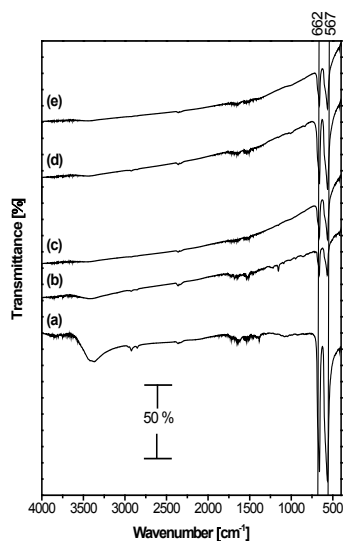


**Figure 7.** FTIR spectra of un-promoted (a); and alkali-promoted (Li<sup>+</sup> (b), Na<sup>+</sup> (c), K<sup>+</sup> (d), and Cs<sup>+</sup> (e)) Co<sub>3</sub>O<sub>4</sub> catalysts having alkali/cobalt ratio of 0.05 being calcined at 400 °C.

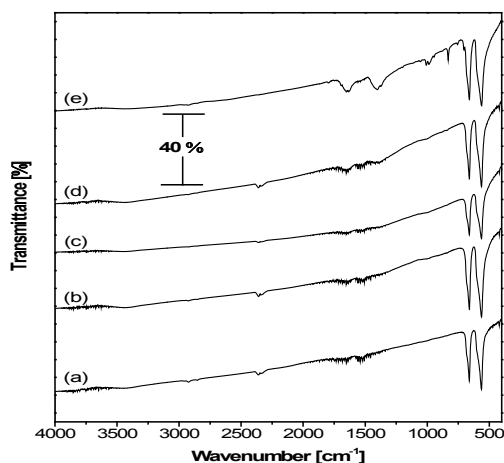


**Figure 8.** FTIR spectra of Cs/Co<sub>3</sub>O<sub>4</sub> catalyst, being calcined at 400 °C at a cesium/cobalt molar ratios of 0.0125 (a), 0.025 (b), 0.05 (c), 0.1 (d), and 0.2 (e).

**Figure 9** shows the FTIR spectra of cesium doped Co<sub>3</sub>O<sub>4</sub> catalysts (Cs/Co<sup>2+</sup> ratio of 0.025) being calcined at 400-700 °C temperature range. Inspection of this figure revealed the co-existence of absorption due to cobalt oxide spinel, carbonate anion, and water molecules. With increasing the calcination temperature the bands related to carbonate anion and water molecules are disappeared.

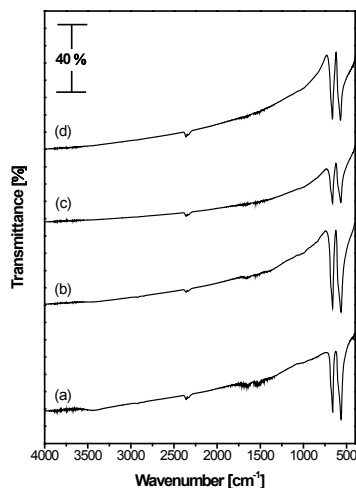


**Figure 9.** FTIR spectra of Cs/Co<sub>3</sub>O<sub>4</sub> (having Cs/Co ratio of 0.025) catalyst being calcined at 400 (a), 500 (b), 600 (c) and 700 (d) °C.

## Catalytic Decomposition of N<sub>2</sub>O

**Figure 10** shows the dependence of the steady-state conversion of N<sub>2</sub>O on the reactor temperature for pure and alkali-doped (where alkali cation/Co=0.05) nano-crystalline Co<sub>3</sub>O<sub>4</sub> catalysts calcined at 400 °C. All the alkali promoted catalysts exhibit a higher N<sub>2</sub>O decomposition activity (T<sub>50</sub> values of 351, 270, 260, and 253 °C for the Li-, K-, Na-, and Cs-promoted catalysts, respectively) compared with that of the un-promoted Co<sub>3</sub>O<sub>4</sub> (T<sub>50</sub>=387 °C). In other words, the activity order is: un-promoted<Li<Na<K<Cs at reaction temperature of 350 °C with N<sub>2</sub>O conversion of 20.57, 48.2, 92.2, 98, and 99.6%, respectively. It is worth noting that for the most active sample Cs–Co<sub>3</sub>O<sub>4</sub>, the N<sub>2</sub>O decomposition starts at a temperature as low as 150 °C and the practically full conversion is reached already at the target temperature of 350 °C. In our case the promotional effect of cesium is superior to that of the other cations reported previously [37,38,43].

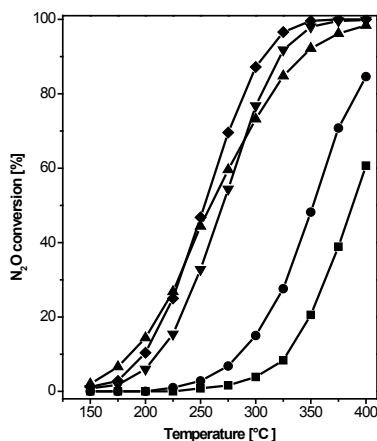
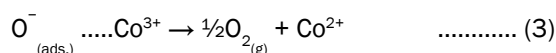
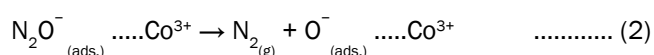
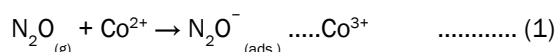


**Figure 10.** Dependence of N<sub>2</sub>O conversion on the reactor temperature for pure nano-crystalline Co<sub>3</sub>O<sub>4</sub> catalyst (■) (prepared using urea/cobalt nitrate ratio of 8 and refluxed for 12 h) and doped with Li (●), Na (▲), K (▼), and Cs (◆) having alkali/cobalt molar ratio of 0.05 and being calcined at 400 °C.

The mechanism of the reaction between N<sub>2</sub>O and the catalysts active centers is generally thought to be a charge donation from the catalyst to the antibonding orbitals of N<sub>2</sub>O, which destabilizes the N–O bond and leads to scission [5]. Therefore, electron charge transfer from the metal ion to the N<sub>2</sub>O molecule is a crucial step for N<sub>2</sub>O decomposition [25]. Electron transfer occurs from a low oxidation state metal cation, which then increases its oxidation state. The recoverability of the ion from a high to a low oxidation state is also important for the regeneration of the active centers. Accordingly, the activity of the Co<sub>3</sub>O<sub>4</sub> oxide spinel is attributed to the coexistence of a Co<sup>2+</sup>-Co<sup>3+</sup> ion pair because of a facile one electron transfer between these ions during N<sub>2</sub>O decomposition, as shown in the following mechanism [25]:



In this mechanism, Eq. 1 is plausible since N<sub>2</sub>O has positive electron affinity of 0.3–0.8 eV [44]. The existence of N<sub>2</sub>O<sup>-</sup> species was confirmed throughout infrared spectra of adsorbed N<sub>2</sub>O on chromia [45]. In addition, the formation of O<sup>-</sup> species (Eq. 2) was identified by ESR studies during N<sub>2</sub>O decomposition over CoO–MgO catalysts [46]. Generally, N<sub>2</sub>O can be adsorbed onto the catalyst surface either through oxygen or nitrogen atoms [7]. Adsorption via oxygen atom would increase the N–N bond order and decreases the bond order between N–O atoms leading to the formation of nitrogen molecule and adsorbed oxygen atom (Eqs. 1,2). On the other hand, N<sub>2</sub>O adsorption via its nitrogen end results in an increase in the bond order between nitrogen and oxygen atoms while decreasing the bond order of the two nitrogen atoms giving NO molecule as a reaction product. This is in a good agreement with the proposed mechanism, where no NO was detected in the reactor outlet (see Sect. 2.3).

Dell *et al.* [47] correlated the N<sub>2</sub>O decomposition activity of a series of metallic oxides with their semi-conductivity behavior. Based on their classification, the highest activity was observed over *p*-type semi-conductors whereas the lowest activity was correlated with *n*-type semi-conductors. Because Co<sub>3</sub>O<sub>4</sub> is a *p*-type semi-conductor [25], this could be another reason for its N<sub>2</sub>O decomposition activity.

**Figure 11** shows the DTA thermograms obtained by heating the 400 °C calcined pure and alkali-doped (where alkali cation/Co=0.05) nano-crystalline Co<sub>3</sub>O<sub>4</sub> catalysts in air to 1000 °C. For pure nano-crystalline Co<sub>3</sub>O<sub>4</sub>, one sharp endothermic peak was found at 915 °C. This peak is attributed to the thermal reduction of Co<sup>3+</sup> to Co<sup>2+</sup>. The introduction of alkali-cations leads to a continuous shift of this peak toward lower temperature in this order: Cs<K<Na<Li<un-doped. For Cs/Co<sub>3</sub>O<sub>4</sub> the maximum of this peak is at about 877 °C. This peak becomes broader with the addition of alkali-cations. It has been reported that the role of alkali cations in the increase of N<sub>2</sub>O decomposition activity is to enhance the Co<sup>3+</sup> to Co<sup>2+</sup> reduction for the cobalt based catalysts,

i.e., the regeneration of  $\text{Co}^{2+}$  ions that are required for  $\text{N}_2\text{O}$  adsorption and subsequent decomposition [36,39]. Based on the data shown in **Figure 11**, it is plausible to suggest that the role of the added alkali-cations is to enhance the  $\text{Co}^{3+}$  to  $\text{Co}^{2+}$  reduction under catalytic conditions and thus increases the catalytic activity. Moreover, in the open literature there are some particularly important contributions about the influence of catalysts crystallites sizes on their activity. Recently, Abu-Zied [11] reported an inverse relationship for Ag crystallite size and  $\text{N}_2\text{O}$  decomposition activity for a series of  $\text{Ag}/\text{Al}_x\text{Fe}_{2-x}\text{O}_3$  catalysts. In addition, Abu-Zied *et al.* demonstrated that the highest  $\text{N}_2\text{O}$  decomposition activity is obtained over catalysts that have a lower  $\text{Co}_3\text{O}_4$  crystallite size for a series of  $\text{SrCO}_3$ - and  $\text{BaCO}_3$ - $\text{Co}_3\text{O}_4$  catalysts [25]. **Table 1** reveals that the addition of alkali-cations from Li to Cs is accompanied by a continuous decrease in catalyst crystallite size. Therefore, the highest activity of the cesium-containing catalyst can be related, also, to its lower crystallite size. Finally and based on the above discussion, the observed higher  $\text{N}_2\text{O}$  decomposition activity of  $\text{Cs}/\text{Co}_3\text{O}_4$  could be due to: (i) its small crystallite size, (ii) the change in the electronic properties of the  $\text{Co}_3\text{O}_4$  as a result of adding Cesium, and (iii) the semi-conductivity character of  $\text{Co}_3\text{O}_4$  since it is known to be a *p*-type semi-conductor. Accordingly, our study was extended to investigate the influence of changing the Cs/Co ratio towards  $\text{N}_2\text{O}$  decomposition activity.

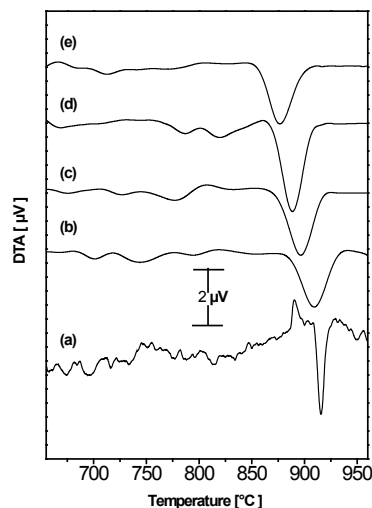


**Figure 11.** DTA comparison between un-doped (a); and alkali-doped ( $\text{Li}^+$  (b),  $\text{Na}^+$  (c),  $\text{K}^+$  (d), and  $\text{Cs}^+$  (e))  $\text{Co}_3\text{O}_4$  catalysts having alkali/cobalt ratio of 0.05 being calcined at  $400^\circ\text{C}$ .

**Figure 12a** depicts the dependence of  $\text{N}_2\text{O}$  conversion on the reactor temperature for nano-crystalline  $\text{Co}_3\text{O}_4$  and its cesium containing  $\text{Co}_3\text{O}_4$  catalysts (where  $\text{Cs}/\text{Co}=0.0125, 0.025, 0.05, 0.10,$  and  $0.20$ ) being calcined at  $400^\circ\text{C}$ . From the inspection of this figure it appears that, over the whole temperature range Cs-doping even at a small ratio ( $\text{Cs}/\text{Co}=0.0125$ ) results in a noticeable increase in activity. A further increase in the  $\text{Cs}/\text{Co}$  ratio is accompanied by a continuous increase in activity until  $\text{Cs}/\text{Co}=0.025$ . After this ratio a continuous decrease in activity is obtained. However, all the Cs-doped catalysts have higher activity compared with the un-doped nano-crystalline  $\text{Co}_3\text{O}_4$  catalyst.

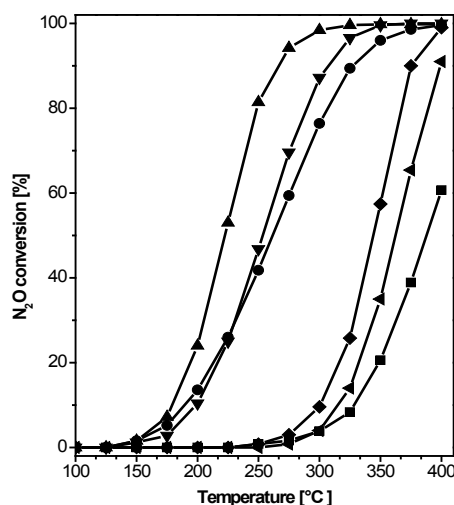


**Figure 12a:** Dependence of  $\text{N}_2\text{O}$  conversion on the reactor temperature for pure nano-crystalline  $\text{Co}_3\text{O}_4$  catalyst ( $\blacksquare$ ) and doped with cesium ( $\text{Cs}/\text{Co}=0.0125$  ( $\bullet$ ),  $0.025$  ( $\blacktriangle$ ),  $0.05$  ( $\blacktriangledown$ ),  $0.10$  ( $\blacklozenge$ ), and  $0.20$  ( $\blacktriangleleft$ )) prepared using urea/cobalt nitrate molar ratio of 8, reflux time 12 h, and being calcined at  $400^\circ\text{C}$ .

**Figure 12b** shows the variation of the temperature of 50%  $\text{N}_2\text{O}$  conversion,  $T_{50}$ , with the  $\text{Cs}/\text{Co}$  molar ratio for cesium doped nano-crystalline  $\text{Co}_3\text{O}_4$  catalysts being calcined at  $400^\circ\text{C}$ . From this figure, the most pronounced effect, as gauged by the 50% conversion temperature, is observed for  $\text{Cs}/\text{Co} 0.025$ , ( $\Delta T_{50\%} = T_{50\%}(\text{un-promoted}) - T_{50\%}(\text{alkali promoted}) = 165^\circ\text{C}$ ); for  $\text{Cs}/$

Co having a molar ratio of 0.05 it drops to  $\Delta T_{50\%} = 134^\circ\text{C}$ . Further increase in cesium ratio to 0.1 was accompanied by shift in  $\Delta T_{50\%}$  value towards higher temperatures by  $120^\circ\text{C}$  on average, i.e.,  $\Delta T_{50\%} = 43^\circ\text{C}$ , whereas for Cs/Co having molar ratio of 0.20  $\Delta T_{50\%} = 24^\circ\text{C}$ . It is noteworthy that, for the most active sample  $\text{Cs}_{0.025}\text{-Co}_3\text{O}_4$ , the  $\text{N}_2\text{O}$  decomposition starts at a temperature as low as  $100^\circ\text{C}$  and the practically full conversion is reached already below the target temperature of  $350^\circ\text{C}$ .

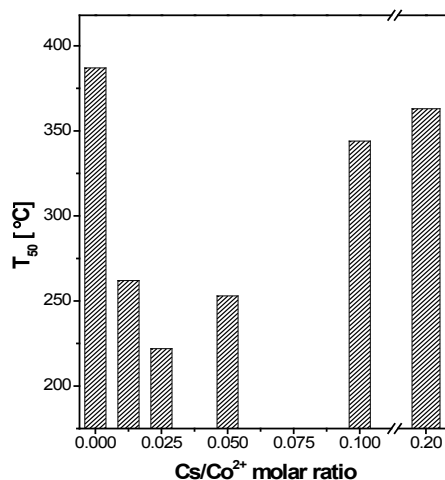


**Figure 12b:** Dependence of T50 on the Cs/Co molar ratio for cesium doped nano-crystalline Co3O4 catalysts prepared using urea/cobalt nitrate molar ratio of 8, reflux time 12 h, and being calcined at  $400^\circ\text{C}$ .

In a series of Cs promoted  $\text{Co}_3\text{O}_4$  catalysts and tested their activity towards direct decomposition of  $\text{N}_2\text{O}$ , it was found that, Cs promoted  $\text{Co}_3\text{O}_4$  catalysts exhibit higher activity for the decomposition of  $\text{N}_2\text{O}$  compared to bulk  $\text{Co}_3\text{O}_4$  also in the presence of oxygen and steam in the feed stream [40]. The catalyst with Cs/Co ratio of 0.05 showed highest activity. The enhancement in catalytic activity of the Cs promoted catalysts was attributed to the change in the electronic properties of  $\text{Co}_3\text{O}_4$  which, in turn, facilitate desorption of oxygen during the reaction. It was demonstrated, based on TPR results, that the presence of small amount of Cs is effective in stabilizing the lower oxidation state of Co due to the interaction between Cs and  $\text{Co}_3\text{O}_4$ , which promotes the reduction of  $\text{Co}^{3+}$  to  $\text{Co}^{2+}$ . At high Cs content, it appears that Cs migrates to Co surface leading to reduction inhibiting counter effect. Concurrently, it is suggested that the easy release of oxygen might be due to the weakening of Co–O bond in the presence of alkali cations [48]. Thus, the early desorption of  $\text{O}_2$  in the case of Cs promoted catalysts might be the reason for its high activity at low reaction temperatures.

Thus, in the light of this interesting literature data, it is plausible to suggest that the enhancement effect of the added cesium cations, during  $\text{N}_2\text{O}$  decomposition over  $\text{Co}_3\text{O}_4$  catalyst, could be also related to the electronic interaction induced by these cations. Such interaction produces electron rich cobalt species that can donate electrons to  $\text{N}_2\text{O}$  molecules leading to the weakening of the N–O bond, thus increasing  $\text{N}_2\text{O}$  decomposition activity. In addition,  $\text{Cs/Co}_3\text{O}_4$  having Cs/Co 0.025 exhibits the lowest crystallite size and the highest  $S_{\text{BET}}$  values among the catalysts of this series. Therefore, as was mentioned above, the observed higher activity of this catalyst (Figure 12a) could be, also, related to its lower crystallite size and higher surface area. Considering the activity decrease with cesium content increase, Pasha *et al.* [40] investigated cesium-promoted  $\text{Co}_3\text{O}_4$  and related the observed decrease in activity for the catalysts with a Cs/Co > 0.05 to the Hedvall effect [49]. In addition, from Table 1, it was shown that increasing the Cs/Co molar ratio from 0.025 to 0.20 leads to a continuous decrease the surface area as well as increase in the crystallite size. Therefore, we may, also, relate negative effect of Cs in promoting the nano-crystalline  $\text{Co}_3\text{O}_4$  activity to its role in decreasing the catalysts surface areas as well as increasing the crystallite sizes.

From Figure 12a it was found that the best performance of cesium promoted nano-crystalline  $\text{Co}_3\text{O}_4$  catalyst is that having Cs/Co ratio of 0.025. Accordingly, we have decided to check the influence of increasing the calcination temperature on its activity. The influence of calcination temperature on the  $\text{N}_2\text{O}$  decomposition activity was reported by many research groups [7,11,25,50] where the observed decrease in activity to BET surface area is correlated to the increase in the calcination temperature.

Figure 13 depicts the dependence of  $\text{N}_2\text{O}$  conversion on the reactor temperature over the cesium containing  $\text{Co}_3\text{O}_4$  catalysts (where Cs/Co=0.025) being calcined at 400, 500, 600, and  $700^\circ\text{C}$ . From a close inspection of this figure one can easily abstract the following points: (i) the onset of the reaction starts at 150, 250, 275, and  $375^\circ\text{C}$  over  $\text{Cs}_{0.025}\text{-Co}_3\text{O}_4$  catalysts calcined at 400, 500, 600, and  $700^\circ\text{C}$ , respectively. (ii) The catalyst calcined at  $400^\circ\text{C}$  exhibit the higher activity than that catalysts calcined at high temperatures (i.e., 500, 600, and  $700^\circ\text{C}$ ). (iii) The maximum  $\text{N}_2\text{O}$  decomposition activity, 100%, was obtained over  $\text{Cs}_{0.025}\text{-Co}_3\text{O}_4$  catalysts calcined at  $400^\circ\text{C}$ , at reaction temperature of  $350^\circ\text{C}$ . (iv) The  $T_{50}$  (temperature of 50% decomposition) showed a shift by 115, 165, and  $205^\circ\text{C}$  to higher temperature upon raising the calcination temperature from 400 to 500, 600, and  $700^\circ\text{C}$ , respectively. From Table 1, it was shown that with the increase in the calcination temperature  $S_{\text{BET}}$  surface area showed a sharp continuous decrease. The  $S_{\text{BET}}$  values decreased, from 34 to  $2.7\text{ m}^2\cdot\text{g}^{-1}$ , as a result of raising the calcination temperature from 400 up to  $700^\circ\text{C}$ . In addition, it was shown that the crystallite size of  $\text{Cs/Co}_3\text{O}_4$  is increased with increasing the calcination temperature

from 400 to 700 °C. Such effect is a direct response of sintering effects which predominated at high temperatures. Thus, one can state safely that the observed dramatic activity decrease accompanying the calcination temperature rise from 400 to 700 °C is attributed to the obtained crystallite size increase as well as the sharp surface area decrease. This, in turn, is accompanied by a decrease in the surface concentration of the  $\text{Co}^{3+}\text{-Co}^{2+}$  redox couple necessary for the  $\text{N}_2\text{O}$  initiation and decomposition.

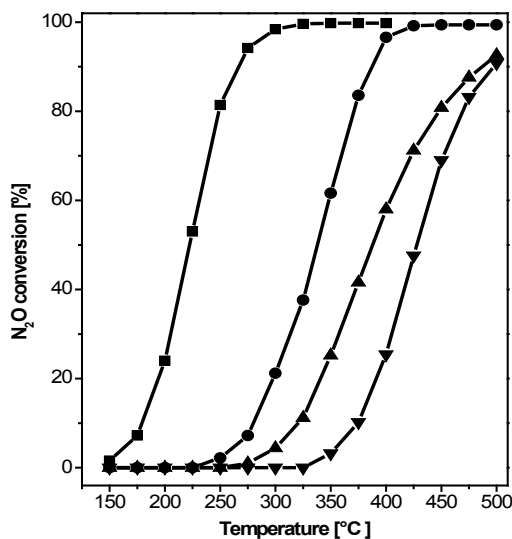


**Figure 13:** Dependence of  $\text{N}_2\text{O}$  conversion on the reactor temperature over cesium doped nano-crystalline  $\text{Co}_3\text{O}_4$  catalysts (prepared using urea/cobalt nitrate molar ratio of 8 and refluxed time 12 h) having Cs/Co molar ratio of 0.025 which are calcined at 400 (■), 500 (●), 600 (▲) and 700 (▼) °C.

## CONCLUSIONS

The present investigation includes, studying the promotional effect of doping alkali cations (Li, Na, K, and Cs) on the catalytic activity of nano-crystalline  $\text{Co}_3\text{O}_4$ , prepared via combustion method, in  $\text{N}_2\text{O}$  decomposition. The sequence of the promotional effect was found to be: un-promoted < Li < Na < K < Cs-promoted catalyst. The reason for the increase in activity for the added alkali cations was electronic in nature. Changing the Cs/Co ratio revealed that the maximum activity was obtained over the catalyst with a Cs/Co of 0.025. At higher Cs/Co ratios, a continuous decrease in activity was observed. The observed decrease in activity for the catalysts with Cs/Co > 0.025 is related to the crystallite size increases and  $S_{\text{BET}}$  decreases.

## ACKNOWLEDGMENTS

The authors would like to gratefully acknowledge the Deutscher Akademischer Austausch Dienst (DAAD) for granting us the use of gas analyzers for these experiments.

## REFERENCES

- Centi G, Perathoner S., Vazzana F, Marella M, Tomaselli M, et al. Novel catalysts and catalytic technologies for  $\text{N}_2\text{O}$  removal from industrial emissions containing  $\text{O}_2$ ,  $\text{H}_2\text{O}$  and  $\text{SO}_2$ , *Adv Environ Res* 2000; 4: 325-338.
- Thiemens MH, Troglor WC. Nylon production: an unknown source of atmospheric nitrous oxide. *Science* 1991; 251: 932-934.
- Pérez-Ramírez J, Kapteij F, Schöffel K, Moulijn JA. Formation and control of  $\text{N}_2\text{O}$  in nitric acid production Where do we stand today? *Appl Catal B Env* 2003; 44: 117-151.
- Troglor WC. Physical properties and mechanisms of formation of nitrous oxide. *Coord Chem Rev* 1999; 187: 303-327.
- Kapteijn F, Rodriguez-Mirasol J, Moulijn JA. Heterogeneous catalytic decomposition of nitrous oxide. *Appl Catal B Env* 1996; 9: 25-64.
- Centi G, Galli A, Montanari B, Perathoner S, Vaccari A. Catalytic decomposition of  $\text{N}_2\text{O}$  over metal and transition metal containing oxides and zeolites. Role of some variables on reactivity. *Catal Today* 1997; 35: 113-120.
- Asano K, Ohnishi C, Iwamoto S, Shioya Y, Inoue M. Potassium-doped  $\text{Co}_3\text{O}_4$  catalyst for direct decomposition of  $\text{N}_2\text{O}$ . *Appl Catal B Env* 2008; 78: 242-249.
- Kim SS, Lee SJ, Hong SC. Effect of  $\text{CeO}_2$  addition to  $\text{Rh}/\text{Al}_2\text{O}_3$  catalyst on  $\text{N}_2\text{O}$  decomposition. *Chem Eng J* 2011; 169: 173-179.
- Mansoure TH, Makhoulf MT, Abu-Zied BM. Rapid preparation, characterization and catalytic decomposition of  $\text{N}_2\text{O}$  over pure and alkali-doped  $\text{Co}_3\text{O}_4/\text{MCM-41}$  nano-composites. *J Nanomed Nanotechol* 2012; 3: 118

10. Parres-Esclapez S, Illán-Gómez MJ, Salinas-Martínez de Lecea C, Bueno-López A. Preparation and characterisation of  $\gamma$ - $\text{Al}_2\text{O}_3$  particles-supported  $\text{Rh}/\text{Ce}_{0.9}\text{Pr}_{0.1}\text{O}_2$  catalyst for  $\text{N}_2\text{O}$  decomposition in the presence of  $\text{O}_2$ ,  $\text{H}_2\text{O}$  and  $\text{NO}_x$ . *Int J Greenhouse Gas Control* 2012; 11: 251-261.
11. Abu-Zied BBM. Oxygen evolution over  $\text{Ag}/\text{Fe}_x\text{Al}_{2-x}\text{O}_3$  ( $0.0 \leq x \leq 2.0$ ) catalysts via  $\text{N}_2\text{O}$  and  $\text{H}_2\text{O}_2$  decomposition. *App Catal A Gen* 2008; 334: 234-242.
12. Yan-Fei P, Ming F, Xian C, Xiu-Feng X. Catalytic activity of alkali metal doped Cu-Al mixed oxides for  $\text{N}_2\text{O}$  decomposition in the presence of oxygen. *J Fuel Chem Technol* 2012; 40: 601-607.
13. Basahel SN, Abd El-Maksod IH, Abu-Zied BM, Mokhtar M. Effect of  $\text{Zr}^{4+}$  doping on the stabilization of ZnCo-mixed oxide spinel system and its catalytic activity towards  $\text{N}_2\text{O}$  decomposition. *J Alloys Comp* 2010; 493: 630-635.
14. Obalová L, Maniak G, Karásková K, Kovanda F, Kotarba A. Electronic nature of potassium promotion effect in Co-Mn-Al mixed oxide on the catalytic decomposition of  $\text{N}_2\text{O}$ . *Catal Commun* 2011; 12: 1055-1058.
15. Wilczkowska E, Krawczyk K, Petryk J, Sobczak JW, Kaszukur Z. Direct nitrous oxide decomposition with a cobalt oxide catalyst. *Appl Catal A Gen* 2010; 389: 165-172.
16. Kögel M, Abu-Zied BM, Schwefer M, Turek T. The effect of  $\text{NO}_x$  on the catalytic decomposition of nitrous oxide over Fe-MFI zeolites. *Catal Commun* 2011; 2: 273-276.
17. Abu-Zied BM, Schwieger W. Self oscillatory behaviour in  $\text{N}_2\text{O}$  decomposition over Co-ZSM-5 catalysts. *App Catal B Env* 2009; 85: 120-130.
18. Abu-Zied BM, Schwieger W, Unger A. Nitrous oxide decomposition over transition metal exchanged ZSM-5 zeolites prepared by the solid-state ion-exchange method, *Appl Catal B Env* 2008; 84: 277-288.
19. Abu-Zied BM.  $\text{Cu}^{2+}$ -acetate exchanged X zeolites: Preparation, characterization and  $\text{N}_2\text{O}$  decomposition activity. *Micropor Mesopor Mat* 2011; 139: 59-66.
20. Park J, Shen X, Wang G. Solvothermal synthesis and gas-sensing performance of  $\text{Co}_3\text{O}_4$  hollow nanospheres. *Sensor Actuat B* 2009; 136: 494-498.
21. Yu Y, Takei T, Ohashi H, He H, Zhang X, et al. Pretreatments of  $\text{Co}_3\text{O}_4$  at moderate temperature for CO oxidation at  $-80^\circ\text{C}$ . *J Catal* 2009; 267: 121-128.
22. Ding Y, Zhang P, Long Z, Jiang Y, Huang J, et al. Synthesis and electrochemical properties of  $\text{Co}_3\text{O}_4$  nanofibers as anode materials for lithium-ion batteries. *Mater Lett*; 62: 3410-3412.
23. C.B. Wang, C.C. Lee, J.L.Bi, J.Y. Siang, J.Y. Liu, C.T. Yeh, Study on the steam reforming of ethanol over cobalt oxides, *Catal. Today* 146 (2009) 76-81.
24. Solsona B, García T, Hutchings GJ, Taylo SH, Makkee M. TAP reactor study of the deep oxidation of propane using cobalt oxide and gold-containing cobalt oxide catalysts. *Appl Catal A Gen* 2009; 365: 222-230.
25. Abu-Zied BM, Soliman SA. Nitrous Oxide Decomposition Over  $\text{MCO}_3-\text{Co}_3\text{O}_4$  ( $\text{M} = \text{Ca}, \text{Sr}, \text{Ba}$ ) Catalysts. *Catal Lett* 2009; 132: 299-310.
26. Petryk J, Kołakowska E. Cobalt oxide catalysts for ammonia oxidation activated with cerium and lanthanum. *Appl Catal B Env* 2000; 24: 121-128.
27. Xie R, Li D, Hou B, Wang J, Jia L, et al. Solvothermally derived  $\text{Co}_3\text{O}_4@m\text{-SiO}_2$  nanocomposites for Fischer-Tropsch synthesis. *Catal Commun* 2011; 12: 380-383.
28. Deraz NM. Catalytic decomposition of  $\text{H}_2\text{O}_2$  on promoted cobaltic oxide catalysts. *Mater Lett* 2002; 57: 914-920.
29. Makhlof MT, Abu-Zied BM, Mansoure TH. Effect of calcination temperature on the  $\text{H}_2\text{O}_2$  decomposition activity of nanocrystalline  $\text{Co}_3\text{O}_4$  prepared by combustion method. *Appl Surf Sci* 2013; 274: 45-52.
30. Jayatissa AH, Guo K, Jayasuriya AC, Gupta T. Fabrication of nanocrystalline cobalt oxide via sol-gel coating. *Mater Sci and Eng B* 2007; 144: 69-72.
31. Teng Y, Yamamoto S, Kusano Y, Azuma M, Shimakawa Y. One-pot hydrothermal synthesis of uniformly cubic  $\text{Co}_3\text{O}_4$  nanocrystals. *Mater Lett* 2010; 64: 239-242.
32. Morsy SMI, Shaban SA, Ibrahim AM, Selim MM. Characterization of cobalt oxide nanocatalysts prepared by microemulsion with different surfactants, reduction by hydrazine and mechanochemical method. *J Alloys Comp* 2009; 486: 83-87.
33. Lai TL, Lai YL, Lee CC, Shu CC, Wang CB. Microwave-assisted rapid fabrication of  $\text{Co}_3\text{O}_4$  nanorods and application to the degradation of phenol. *Catal Today* 2008; 131: 105-110.
34. Makhlof MTH, Abu-Zied BM, Mansoure TH. Direct Fabrication of Cobalt Oxide Nano-particles Employing Glycine as a Combustion Fuel. *Phys Chem* 2012; 2 86.
35. Makhlof MTH, Abu-Zied BM, Mansoure TH. Direct Fabrication of Cobalt Oxide Nanoparticles Employing Sucrose as a

- Combustion Fuel, J Nanoparticles (2013) (<http://dx.doi.org/10.1155/2013/384350>).
36. Cheng H, Huang Y, Wang A, Li L, Wang X, et al. N<sub>2</sub>O decomposition over K-promoted Co-Al catalysts prepared from hydrotalcite-like precursors. *Appl Catal B Env* 2009; 89: 391-397.
  37. Stelmachowski P, Maniak G, Kotarba A, Sojka Z. Strong electronic promotion of Co<sub>3</sub>O<sub>4</sub> towards N<sub>2</sub>O decomposition by surface alkali dopants. *Catal Commun* 2009; 10: 1062-1065.
  38. Ohnishi C, Asano K, Iwamoto S, Chikama K, Inoue M. Alkali-doped Co<sub>3</sub>O<sub>4</sub> catalysts for direct decomposition of N<sub>2</sub>O in the presence of oxygen. *Catal Today* 2007; 120: 145-150.
  39. Xue L, Zhang C, He H, Teraoka Y. Promotion effect of residual K on the decomposition of N<sub>2</sub>O over cobalt-cerium mixed oxide catalyst. *Catal Today* 2007; 126: 449-455.
  40. Pasha N, Lingaiah N, Babu NS, Reddy PSSS, Prasad PSSS. Studies on cesium doped cobalt oxide catalysts for direct N<sub>2</sub>O decomposition in the presence of oxygen and steam. *Catal Commun* 2008; 10: 132-136.
  41. Zasada F, Stelmachowski P, Maniak G, Paul JF, Kotarba A, et al. Potassium Promotion of Cobalt Spinel Catalyst for N<sub>2</sub>O Decomposition-Accounted by Work Function Measurements and DFT Modelling. *Catal Lett* 2009; 127: 126-131.
  42. Stelmachowski P, Zasada F, Maniak G, Granger P, Inger M, et al. Optimization of Multicomponent Cobalt Spinel Catalyst for N<sub>2</sub>O Abatement from Nitric Acid Plant Tail Gases: Laboratory and Pilot Plant Studies. *Catal Lett* 2009; 130: 637-641.
  43. Abu-Zied BM. Nitrous Oxide Decomposition over Alkali-Promoted Magnesium Cobaltite Catalysts. *Chin J Catal* 2011; 32: 264-272.
  44. Tschumper GS, Schaefer HF. Predicting electron affinities with density functional theory: Some positive results for negative ions. *J Chem Phys* 1997; 107: 2529.
  45. Zecchina A, Cerruti L, Borello E. An infrared study of nitrous oxide adsorption on  $\alpha$ -chromia, *J Catal* 1972; 25: 55-64.
  46. Indovina V, Cordischil D, Occhiuzzi M, Rieti A. Decomposition of N<sub>2</sub>O on High Surface Area CoO-MgO Catalysts Investigated by Electron Spin Resonance Spectroscopy. *J Chem Soc Faraday Trans* 1979; 75: 2177-2187.
  47. Dell RM, Stone FS, Tiley PF. The decomposition of nitrous oxide on cuprous oxide and other oxide catalysts. *Trans Faraday Soc* 1953; 49: 201-209.
  48. Haneda M, Kintaichi Y, Bion N, Hamada H. Alkali metal-doped cobalt oxide catalysts for NO decomposition. *Appl Catal B* 2003; 46: 473-482.
  49. Hedvall JA. Current Problems of Heterogeneous Catalysis. *Adv Catal* 1956; 8: 1-15.
  50. Alini S, Basile F, Blasioli S, Rinaldi C, Vaccari A. Development of new catalysts for N<sub>2</sub>O-decomposition from adipic acid plant. *Appl Catal B Env* 2007; 70: 323-329.